Research Article

Junfeng Zhang*, Dandan Shi, Qinxin Wang, and Hang Lv

The mechanism of carbon monoxide fluorescence inside a femtosecond laser-induced plasma

https://doi.org/10.1515/phys-2025-0135
received September 02, 2024; accepted January 03, 2025

Abstract: The fluorescence spectrum of CO molecules in intense femtosecond laser fields was studied experimentally. Distinct spectral lines from excited atoms and molecules were identified. Different dependencies on gas pressure were observed for atomic and molecular spectral lines. Analysis indicated that these atomic spectral lines were induced by the TBR process, and those molecular spectral lines were induced by collision-induced excitation with tunneling electrons. This study paves the way for a better understanding of complex plasma processes.

Keywords: femtosecond laser, carbon monoxide, fluorescence, plasma

1 Introduction

As the second most abundant interstellar molecule after hydrogen, carbon monoxide plays very important roles in relevant fields, such as plasma physics, combustion science, and astrophysics [1]. Beyond the Earth, the CO molecules have also been observed in comets, planetary atmospheres, interstellar medium, and the photospheres of the Sun and cooler stars, and usually are employed as probes for atmospheric structure and dynamics [2]. The detection of CO molecules is involved in transition spectroscopy; thus, the fluorescence of CO molecules has been intensively studied both theoretically and experimentally. Most previous studies were performed on spectroscopy and molecular properties [3]; however, plasma still lacks research.

With the development of laser technology, femtosecond laser is found to be an ideal tool for generating plasma, and the dynamic processes become a hot topic for molecules in such intense laser fields. Because there are many possible excitation pathways in laser-induced plasma, the formation mechanism of excited atoms and molecules remains controversial. In a single atom/molecule case, the electrons could be excited by resonance, absorbing single or several photons and populated into excited states [4]. Even under non-resonant conditions, electrons could also be excited into atomic and molecular Rydberg states through frustrated tunneling ionization or multi-photon resonance excitation in intense laser fields [5–7]. Collisions prevail in the laser-induced plasma at high gas pressure. Then, the formation mechanism for the fluorescence of atoms and molecules becomes more complex. Several mechanisms, such as radiative recombination [8], dielectronic recombination, three-body recombination (TBR) [9], and impact excitation by ions or electrons [10], have all been observed in laser-induced plasma. Thus, it is very difficult to identify the formation mechanism of fluorescence in laser-induced plasma.

In this study, we measured the fluorescence spectrum of CO molecules in intense femtosecond laser fields. Numerous spectral lines were observed in the laser-induced plasma. These spectral lines were clearly identified and classified into emission from excited neutral atoms and molecules. By measuring the dependence of fluorescence intensity on gas pressure and laser intensity, combined with the plasma parameters, we studied the formation mechanism of CO molecule fluorescence in laser-induced plasma. Our research indicates that the different excitation mechanisms exist simultaneously, and the identification of the fluorescence mechanism paves the way for further understanding of the dynamic processes in plasma.

2 Experiment setup

The experimental setup used for fluorescence spectrum in femtosecond laser fields is similar to those described in our

* **Corresponding author: Junfeng Zhang**, School of Electrical and Information Engineering, Jilin Engineering Normal University, Changchun, 130052, China, e-mail: 1362255329@qq.com
Dandan Shi, **Qinxin Wang:** School of Electrical and Information Engineering, Jilin Engineering Normal University, Changchun, 130052, China
Hang Lv: Institute of Atomic and Molecular Physics, Jilin University, Changchun, 130012, China

previous studies [11]. The fluorescence spectrum was measured in a 20 cm-long air-tight cell. An oil-free mechanical pump was used to pump the reaction region, providing a base pressure of 0.01 Pa. CO gas was leaked into the cell through an effusive valve. The operating pressure was in the range of 0.1–1,000 Pa, which was carefully controlled by a flowmeter. The femtosecond laser pulses (50 fs, 800 nm, 1 kHz, linearly polarized) from a commercial Ti:sapphire laser system (Libra, Coherent) were introduced into the reaction region by a 25 cm focus lens. At the focus, a neutral density filter was inserted into the laser beam to vary the laser intensity continuously. The fluorescence emitted from these excited atoms and molecules was collected and introduced into an optical fiber laterally. Two kinds of detectors were used to measure the fluorescence at the end of the optical fiber. A whole frequency spectrum of the fluorescence in the range of 350–1,100 nm was recorded using a spectrometer (Ocean Optics, QE Pro). To achieve the decay dynamics of these spectral lines, a monochromator (Zolix, grating: 1,200 grooves/mm) was used in front of the photomultiplier (PMT, Zolix), and the time domain curves were recorded by a data acquisition card (NI 5162). The fluorescence lifetime was obtained by fitting the falling edge of the time domain curve with an exponential function.

3 Results and discussion

Figure 1 shows the fluorescence spectrum of CO molecules at 1,000 Pa with a laser intensity of 2×10^{14} W/cm^2. Numerous atomic spectral lines were observed and numbered in order of the wavenumber. By comparing with the NIST database, these atomic spectral lines are assigned to the radiative transition of neutral carbon and oxygen atoms, as listed in Table 1. Due to the small base pressure, it is certain that the background fluorescence signal from air molecules (O_2) was completely reduced. Besides, a series of equally spaced spectral lines with broad line profiles are also identified and assigned to be the emission of neutral excited CO molecules. The heads of several progressions for $d^3\Delta$ state ($v' = 5, 6, 7$) and $e^3\Sigma^-$ state ($v' = 3, 4$) [12], coincident with the observed spectral lines, are calculated according to the molecular parameters of these electronic states. The major subdivisions of these neutral molecular spectral lines result from the spin-orbit splitting.

To study the fluorescence mechanism of CO molecules, we measured the intensity of these spectral lines as a function of gas pressure. Two different kinds of dependences are observed as the gas pressure increases, indicating that these fluorescence are produced by different mechanisms.

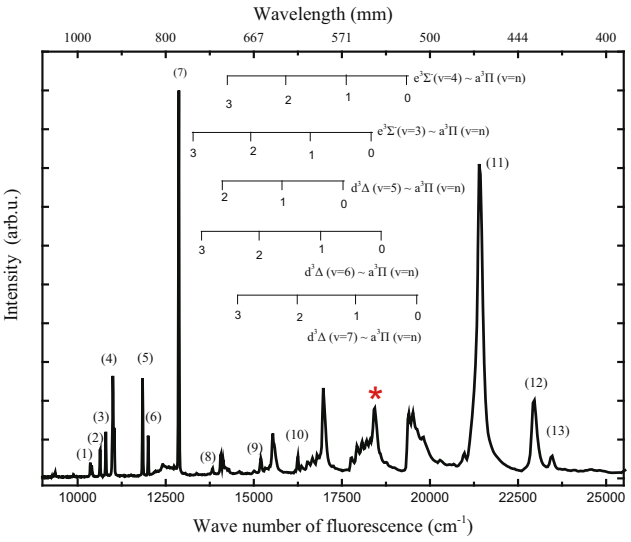

Figure 1: The fluorescence spectrum of CO molecules at 1,000 Pa with a laser intensity of 2×10^{14} W/cm^2. These atomic spectral lines are numbered in order. The heads of several molecular spectral lines of CO molecules are indicated.

Thus, these spectral lines are divided into two parts accordingly. For the first part, some atomic spectral lines (lines nos. 3–5, 7–10, and 13) become visible when the gas pressure is greater than 20 Pa. As an example, the results of C I 658.76 nm (line no. 9) spectral line are shown in Figure 2(a). As shown in the figure, the fluorescence intensity increases with gas pressure, reaches the maxima around 300 Pa of gas pressure, and becomes a constant intensity after that. For the second part, i.e., molecular spectral lines, the results of 542.45 nm ($e^3\Sigma^-$ state of the CO molecule, labeled with red asterisk in Figure 1) are shown in Figure 2(b) as an example. As can be seen, this spectral line emerges until 100 Pa and increases with the gas pressure as a quadratic function, which is different from the abovementioned atomic spectral lines. On the contrary, other atomic spectral lines (line nos 1, 2, 6, 11, and 12) have the same dependence with these molecular spectral lines. Thus, it is supposed that a portion of these excited molecules are not stable, and excited atoms are produced by the neutral dissociation of highly excited molecules [13,14], which then leads to the formation of these atomic spectral lines. Therefore, these atomic spectral lines (line nos 1, 2, 6, 11, and 12) are also viewed as molecular spectral lines in the following part. The lifetimes of atomic (658.76 nm) and molecular (542.45 nm) spectral lines were measured, as shown in Figure 2(c) and (d), respectively. Both of them decrease exponentially with the gas pressure, indicating that the collisions should be considered in this range of gas pressure. The different formation mechanisms of these atomic and molecular spectral lines are discussed in the following section.

Table 1: Identification of neutral atomic spectral lines

Line no.	Wavelength (nm)	Atomic species	Transition
1	965.84	C	$2s^22p3s——2s^22p3p$
2	940.57	C	$2s^22p3s——2s^22p3p$
3	926.08	O	$2s^22p^3(^4S_0)3s——2s^22p^3(^4S_0)3d$
4	909.15	C	$2s^22p3s——2s^22p3p$
5	844.64	O	$2s^22p^3(^4S_0)3s——2s^22p^3(^4S_0)3p$
6	833.51	C	$2s^22p3s——2s^22p3p$
7	777.19	O	$2s^22p^3(^4S_0)3s——2s^22p^3(^4S_0)3p$
8	724.13	C	$2s^22p3s——2s^22p6s$
9	658.76	C	$2s^22p3s——2s^22p4d$
10	615.60	O	$2s^22p^3(^4S_0)3p——2s^22p^3(^4S_0)4d$
11	467.67	C	$2s^22p3s——2s^22p4p$
		C	$2s^22p3p——2s^22p$ 15s/14s/13d
12	437.14	C	$2s^22p3s——2s^22p5p$
	436.82	O	$2s^22p^3(^4S_0)3s——2s^22p^3(^4S_0)4p$
13	426.90	C	$2s^22p3s——2s^22p5p$

In plasma, neutral excited atoms are usually produced by the recombination of electrons with the corresponding ions. There are three recombination processes: radiative recombination, dielectronic recombination, and three-body recombination (TBR). In this experiment, the emissions of radiative recombination (*i.e.*, continuous spectrum) and dielectronic recombination (*i.e.*, spectral lines from excited atomic ions) were not observed in Figure 1, and hence, these two mechanisms were excluded. Therefore, the TBR process, whose rate is two orders of magnitude larger than the radiative recombination, is the possible mechanism for the formation of these atomic spectral lines [15,16].

This TBR process could be expressed as

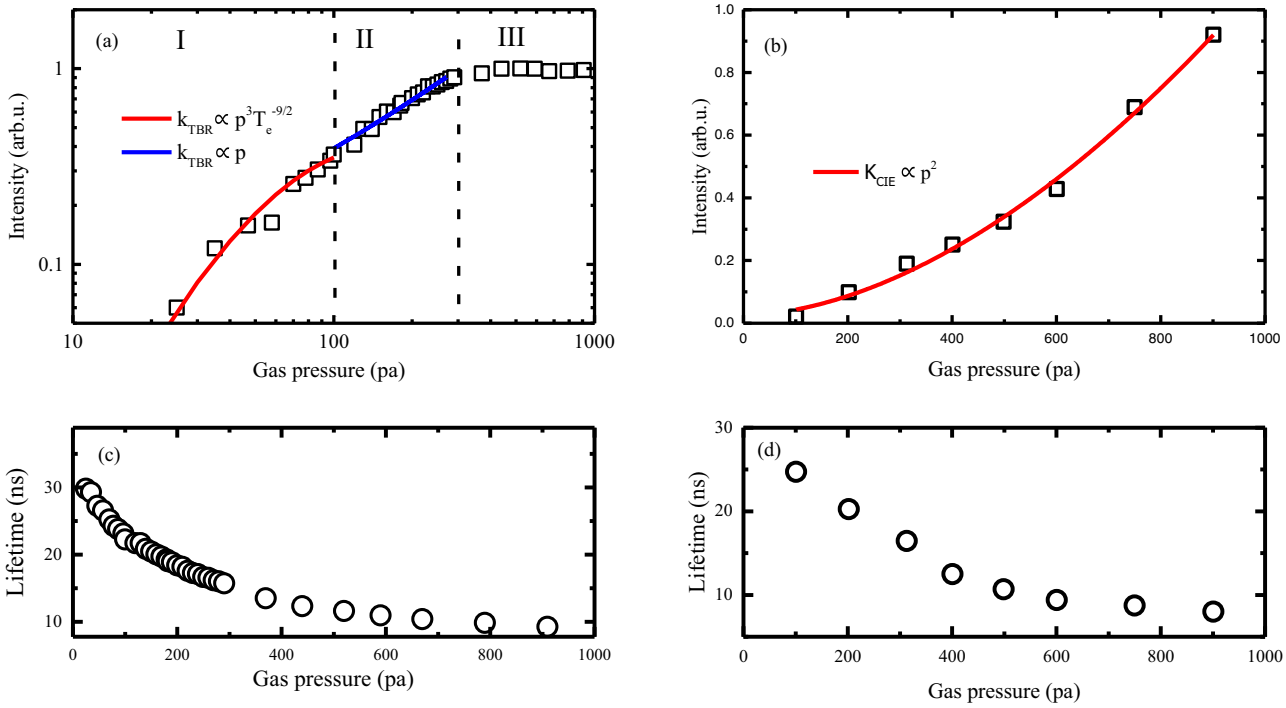

Figure 2: The normalized fluorescence intensity (a) and lifetime (c) as a function of gas pressure for atomic spectral line (658.76 nm) with a laser intensity of 2×10^{14} W/cm^2. The same as (a) and (c) but for molecular spectral line (542.45 nm) are shown in (b) and (d). The solid lines in (a) and (b) are the TBR rate and collision-induced excitation rate as a function of gas pressure (see text).

$$A^+ + e + M \rightarrow A* + M, \quad (1)$$

where ion A^+ (C^+/O^+) would capture an electron and turn into an excited atom A* (C*/O*), and the energy released in the recombination process is obtained by another bystander M. In this experiment, the most possible bystander M is a neutral molecule.

According to Formula (1), the atomic fluorescence intensity is proportional to the TBR rate k_{TBR}, which can be written as

$$k_{TBR} \propto N_{A^+} \times N_e \times N_M \times \sigma_{TBR}, \quad (2)$$

where N_{A^+}, N_e, and N_M are the number density of ions, electrons, and bystanders, respectively. In plasma, the number density of ions N_{A^+} is proportional to the density of electrons N_e, and the number density of bystander N_M linearly depends on the gas pressure. σ_{TBR} is the cross section of the TBR process, which is proportional to $T_e^{-9/2}$, where T_e is the plasma temperature [17,18]. Therefore, the electron density N_e and the plasma temperature T_e are needed for the estimation of the TBR rate k_{TBR}.

In the local thermodynamic equilibrium (LTE) condition, the electron density N_e and plasma temperature T_e could be determined according to the measured fluorescence spectrum; the method is described in the papers [19,20], and the results are shown as a function of gas pressure in Figure 3. In general, both the electron density N_e and plasma temperature T_e linearly increase with gas pressure and reach a maximum of 100 Pa. Actually, there are two production mechanisms for the free electrons in the laser-induced plasma, *i.e.*, strong field tunneling ionization and collision ionization. In the beginning, electrons are produced through tunneling ionization of CO molecules in intense laser fields. Then, the energetic electrons could induce another ionization and produce secondary electrons in the next collision process. This collision ionization would repeat until the laser pulse ends. Compared with the low rate of tunneling ionization (0.1%), almost 40% of CO molecules are ionized at 100 Pa (the electrons density is 1×10^{16} cm^{-3}, and the initial number density of CO molecules at 100 Pa is about 2.5×10^{16} cm^{-3}), which indicates that most electrons are produced by collision ionization. When the plasma is in the case of LTE, the average kinetic energy is only about 0.4 eV for the secondary electrons with the temperature T_e = 4,500 K [19]. Compared with the tunneling electrons, these secondary electrons with small kinetic energy are easier to capture by atomic ions; therefore, we believe that the electrons in the TBR process were produced through collision ionization.

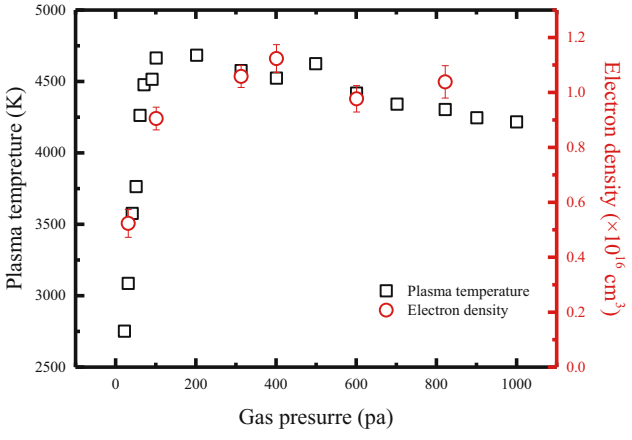

Figure 3: The plasma temperature T_e and electron density N_e as a function of gas pressure at a laser intensity of 2×10^{14} W/cm^2.

In order to confirm the TBR mechanism of these atomic spectral lines, we divide Figure 2(a) into three regions for a detailed discussion. In region I (20–100 Pa), both the electron density N_e and plasma temperature T_e linearly increase with the gas pressure (Figure 3). Then, the dependence of TBR rate k_{TBR} on gas pressure p could be expressed as $p^3 T_e^{-9/2}$, according to Formula (2). The variation tendency of k_{TBR} is shown in Figure 2(a) with red lines by multiplying a coefficient. A good fitting was observed between this variation tendency and the experimental measurements. In Region II (100–300 Pa), both the electron density Ne and plasma temperature T_e change slightly with the gas pressure (Figure 3); the same applies to the number density of atomic ions N_{A^+}. The TBR cross section σ_{TBR}, which is proportional to $T_e^{-9/2}$, is also irrelevant to the gas pressure in this region. Therefore, the TBR rate k_{TBR} is in direct proportion to the gas pressure in this region according to Formula (2), owing to the number density increment of the bystander N_M, and the variation tendency of k_{TBR} in this region is shown in Figure 2(a) with blue lines, which is in line with the experimental observation. As the gas pressure increased, the mean free path in plasma became smaller, and the rate k_{TBR} of the TBR process consumed the free electrons and continued to increase and finally surpassed the collision ionization rate. Finally, an equilibrium is established between the ionization and TBR processes in plasma when the gas pressure is beyond 300 Pa. Therefore, the TBR rate k_{TBR}, as well as the atomic spectral intensity, does not increase further in region III, as shown in Figure 2(a). The full agreement between this TBR rate with the measured atomic fluorescence intensity indicates that the production mechanism of these atomic spectral lines is indeed the TBR process.

As mentioned above, the production mechanism of molecular spectral lines is different from that of atomic

spectral lines. Similar to the excited nitrogen molecules $N_2(C^3\Pi_u)$ inside the laser filaments, there are three possible mechanisms to populate these neutral excited $CO(e^3\Sigma^-)$ molecules: collision-assisted inter-system crossing [CO + mhv → CO*; CO*(ISC) → $CO(e^3\Sigma^-)$], dissociative recombination [21] [CO^{++} CO → $(CO)_2^{++}$; $(CO)_2^{++}$ e → $CO(e^3\Sigma^-)$ + CO], and collision-induced excitation [21,22] [$CO(X^1\Sigma^+)$ + e → $CO(e^3\Sigma^-)$ + e]. In order to study the mechanism of molecular fluorescence, we present the fluorescence intensity dependence of atomic (658.76 nm) and molecular (542.45 nm) spectral lines on laser intensity at 1,000 Pa in Figure 4. The saturation laser intensity of the atomic spectral line is estimated to be 1×10^{14} W/cm^2, which is similar to that of tunneling ionization of CO molecules [23]. This is because all these complicated processes for TBR in plasma start with tunneling ionization. Clearly, the molecular spectral line has the same saturation laser intensity as that of the atomic spectral line. Compared with the TBR process in which CO molecules are ionized, less energy (~8 eV) is needed for the collision-assisted inter-system crossing, in which the electron is excited into an electric state near the $CO(e^3\Sigma^-)$ state. Therefore, if these neutral excited CO molecules are produced through collision-assisted inter-system crossing, a small saturation laser intensity would be expected, which disagrees with the observation in Figure 4. As a result, we exclude this collision-assisted inter-system crossing for the formation mechanism of molecular spectral lines.

Next, we consider the possibility of molecular excitation by dissociative recombination. It should be pointed out that the dissociative recombination was observed at a rather high gas pressure in previous studies (a few thousands of pascal to atmospheric pressure) [21]. While at such a low gas pressure (~100 Pa), the probability of collision between molecules and ions is very low. Furthermore, when the gas pressure is greater than 100 Pa, the number density of CO^+ ion N_{CO^+} and low energy electron N_e (secondary electron produced by collision ionization) are independent of the gas pressure (Figure 3). Only the number density of neutral CO molecules linearly increases with the gas pressure. Therefore, a linear dependence of the dissociative recombination rate on gas pressure is expected, which is inconsistent with the observation in Figure 2(b). Thus, the molecular spectral lines produced through this dissociation recombination should be ruled out in our experiment.

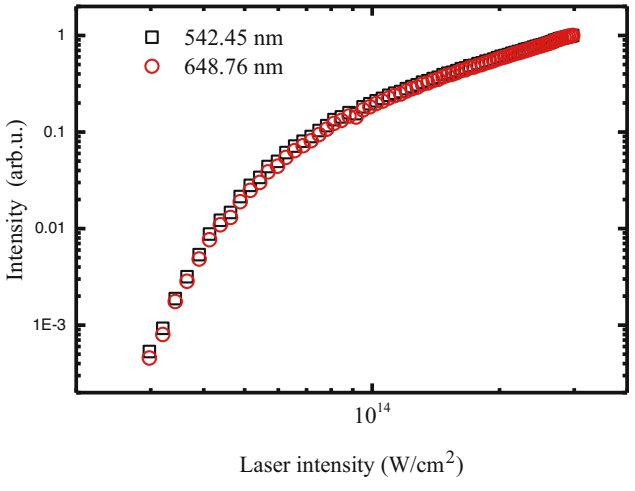

Figure 4: The normalized fluorescence intensities of atomic (658.76 nm) and molecular (542.45 nm) spectral lines as a function of laser intensity.

As a consequence, the formation of neutral excited CO molecules in plasma is attributed to the collision-induced excitation. The molecular fluorescence intensity is proportional to the electron impact excitation rate k_{CIE}, which can be written as

$$k_{CIE} \propto N_{CO} \times N_e \times \sigma_{CIE}, \tag{3}$$

where N_{CO} and N_e are the number density of the ground state molecules and energetic electrons, respectively. σ_{CIE} is the electron collision excitation cross section of CO molecules, which only depend on the kinetic energy of electrons, independent of the gas pressure. As the gas pressure increased, N_{CO} linearly increased accordingly.

Energetic electrons are essential for the collision-induced excitation of CO molecules. Thus, the contribution of secondary electrons to this collision-induced excitation process is quite small. This is because the secondary electrons with a temperature T_e = 4,500 K only have an average kinetic energy of about 0.4 eV. The electron with such small kinetic energy does not cannot excite the CO molecules.

Energetic electrons could be produced in tunneling ionization if the rescattering process is included. Both the number density of neutral molecules N_{CO} and tunneled electrons N_e linearly depend on the gas pressure. The electron impact excitation cross section σ_{CIE} is independent of the gas pressure because the kinetic energy of electrons in tunneling ionization is irrelevant to the gas pressure. According to Formula (3), the fluorescence intensity induced by the collision of tunneled electrons should depend quadratically on the gas pressure, and the variation tendency is shown in Figure 2(b) (red line), which is in line with the observed molecular spectral line. This proves that these molecular spectral lines are produced through collision-induced excitation by energetic tunneling electrons. Due to the small tunneling ionization rate (~0.1%), the number density of tunneling electrons is rather small, leading to a relatively small electron impact excitation rate k_{CIE}; therefore, these molecular spectral lines become visible until the gas pressure is larger than 100 Pa.

4 Determination of the electron density and plasma temperature

Because of the dominance of the collision processes, the plasma should be in local thermal equilibrium (LTE). The criteria of LTE reads $N_e \geq N_{cr} = 1.6 \times 10^{12}\sqrt{T}(\Delta E)^3$ where T (in K) is the plasma temperature, ΔE (in eV) is the energy difference for levels in the transition, and N_{cr} is the critical density for thermal equilibrium. For the spectral line of CI 658.76 nm, inserting $\Delta E \approx 1.88$ eV and a reasonable upper limit estimation of $T \approx 10{,}000$ K, the critical density N_{cr} is calculated to be less than 10^{15} cm^{-3}. This value is much less than the plasma density obtained in Figure 3 (~10^{16} cm^{-3}). This justifies the formation of plasma and the condition of LTE. In thermodynamic equilibrium, the plasma can be fully described by partition functions independent of the excitation mechanism (*e.g.*, by arc, shock tube, plasma jet, or laser).

The electron density and plasma temperature are the two independent parameters that describe the plasma and could be deduced from the fluorescence spectrum. The plasma temperature could be determined by the well-known Boltzmann method from the relative spectral line intensity, provided that the transition probabilities A_{mn} from a given excited state are known. The populations of the excited states follow a Boltzmann distribution, and their relative emissivity ε_{mn} can be given by

$$\ln\left(\frac{\lambda\varepsilon_{mn}}{g_m A_{mn}}\right) = \ln\frac{N(T)}{U(T)} - \frac{E_m}{kT_e},$$

where λ, A_{mn}, and g_m are the wavelength, the transition probability, and the statistical weight for the upper level, respectively; E_m is the excited level energy; T_e is the plasma temperature; k is the Boltzmann constant; $U(T)$ is the partition function, and $N(T)$ is the atomic density. To construct the Boltzmann plot, three atomic lines of O I (line no. 3, 5, 7) are selected, because they are well isolated, having a sufficient signal-to-noise ratio. Moreover, the energy difference of their upper levels is large enough to provide reasonable accuracy. Accordingly, the plasma temperature is determined from the slope of the Boltzmann plot. By repeating this procedure, the plasma temperature is computed as a function of gas pressure, and the results are shown in Figure 3.

The measured line profile originates from different line shifts and broadening mechanisms that can be divided into stark broadening, Doppler broadening, and resonant pressure broadening. Here, the stark broadening prevails, which results from the perturbation of the excited levels of the radiating atoms due to collisions mainly with the plasma electrons, whereas other broadening mechanisms are negligible [24]. In quasi-static approximation, the plasma density, associated with electron impact, is proportional to the FWHM of the stark broadening line width $\Delta\lambda = 2\omega\left(\frac{N_e}{10^{16}}\right)$, where N_e is the plasma density and ω is the electron collision parameter. In general, the electron parameter is weakly dependent on the electron temperature; therefore, $\omega = 1.16$ nm for C I 658.76 nm emission was used in the whole range.

The line profile of CI 658.76 nm was measured as a function of gas pressure. The instrumental revolution for the monochromator with the 1,200 grooves/mm grating was estimated to be $\Delta\lambda = 0.23$ nm (slit width is 100 μm), which is only a few percent of the CI 658.76 nm line width. Thus, the Stark broadening was corrected by subtracting the $\Delta\lambda$ from the FWHM of the atomic spectral line, which is obtained by fitting the experimental spectral profile with a Lorenz function. Having both the ω and $\Delta\lambda$, the plasma density in the laser-induced plasma could be calculated accordingly, and the results as a function of gas pressure are shown in Figure 3.

5 Conclusion

In summary, the fluorescence spectrum of CO molecules in intense femtosecond laser fields was studied experimentally. Distinct spectral lines from excited atoms and molecules were identified. Different dependencies on gas pressure were observed for atomic and molecular spectral lines. Analysis indicated that these atomic spectral lines were induced by the TBR process, and the molecular spectral lines were induced by collision-induced excitation with tunneling electrons. This study clearly distinguished the different production mechanisms for the fluorescence of CO molecules in laser-induced plasma and paved the way for further understanding of the complicated processes in plasma, such as the air laser and laser filament.

Funding information: This work was supported by the Science and Technology Research Project of Jilin Provincial Department of Education (Grant No. JJKH20240226KJ) and the Jilin Engineering Normal University Scientific Research Project (Grant Nos BSGC202004 and BSKJ201839).

Author contributions: Junfeng Zhang: experimental design, data analysis, and writing; Qinxin Wang and Dandan Shi: assisting Junfeng Zhang with data analysis; Hang Lv: assisting Junfeng Zhang with experimental design and

validation of data analysis. All authors have accepted responsibility for the entire content of this manuscript and approved its submission.

Conflict of interest: The authors state no conflict of interest.

Data availability statement: The datasets generated and/or analyzed during the current study are available from the corresponding author on reasonable request.

References

[1] Estekia K, Predoi-Cross A, Povey C, Ivanov S, Ghoufi A, Thibault F. Room temperature self- and H2-broadened line parameters of carbon monoxide in the first overtone band: Theoretical and revised experimental results. J Quant Spectrosc Radiat Transf. 2017;203:309–24.

[2] Reed ZD, Hodges JT. Line shape parameters of helium-broadened $^{12}C^{16}O$ transitions in the 3 → 0 overtone band near 1.57 μm. J Quant Spectrosc Radiat. 2017;203:300–8.

[3] Madhu Trivikram T, Hakalla R, Heays AN, Niu ML, Scheidegger S, Salumbides EJ. Perturbations in the $A^1\Pi$, v = 0 state of $^{12}C^{18}O$ investigated via complementary spectroscopic techniques. Mol Phys. 2017;115:3178–91.

[4] Bruzzese R, Sasso A, Solimeno S. Multiphoton excitation and ionization of atoms and molecules. La Riv del Nuovo Cimento. 1989;12:1–105.

[5] Hu S, Hao X, Lv H, Liu M, Yang T, Xu H. Quantum dynamics of atomic Rydberg excitation in strong laser fields. Opt Express. 2019;27:31629–43.

[6] Shvetsov-Shilovskia NI, Goreslavskia SP, Popruzhenkoa SV, Beckerb W. Capture into rydberg states and momentum distributions of ionized electrons. Laser Phys. 2009;19:1550.

[7] Nubbemeyer T, Gorling K, Saenz A, Eichmann U, Sandner AW. Strong-field tunneling without ionization. Phys Rev Lett. 2008;101:233001.

[8] Seaton MJ. Radiative recombination of hydrogenic ions. Mon Not R Astron Soc. 1959;119:81–9.

[9] Ticknor C, Rittenhouse ST. Three body recombination of ultracold dipoles to weakly bound dimers. Phys Rev Lett. 2010;105:13201.

[10] Bartschat K. Electron collisions-experiment, theory, and applications. J Phys B At Mol Opt Phys. 2018;51:132001.

[11] Zuo W, Ben S, Lv H, Zhao L, Guo J. Experimental and theoretical study on nonsequential double ionization of carbon disulfide in strong near-IR laser fields. Phys Rev A. 2016;93:53402.

[12] Slanger TG, Black G. Relative electronic transition moments for the triplet system ($d^3\Delta$ to $a^3\Pi$) of CO. J Phys B, At Mol Phys. 1972;5:1988.

[13] Ehresmann A, Demekhin PV, Kielich W, Haar I, Uter MAS. Predominant dissociation of the $CO^*(D^2\Pi)n(d/s)\sigma$ Rydberg states into atomic excited Rydberg fragments with the same effective principal quantum number. J Phys B-At Mol Opt. 2009;42:165103.

[14] Liebel H, Lauer S, Vollweiler F, Muller-Albrecht R, Ehresmann A. Neutral photodissociation of O2 Rydberg states accompanied by changes of the Rydberg electron's quantum numbers n and l. Phys Lett A. 2000;267:357–69.

[15] Forrey CR. Rate of formation of hydrogen molecules by three-body recombination during primordial star formation. Astrophys J. 2013;773:L25.

[16] D'Angelo N. Recombination of ions and electrons. Phys Rev. 1961;121:505.

[17] Mansbach P, Keck J. Monte Carlo trajectory calculations of atomic excitation and ionization by thermal electrons. Phys Rev. 1969;181:275.

[18] Vriens L, Smeets M. Cross-section and rate formulas for electron-impact ionization, excitation, deexcitation, and total depopulation of excited atoms. Phys Rev A. 1980;22:940.

[19] Bernhardt J, Liu W, Théberge F, Xu HL, Daigle JF. Spectroscopic analysis of femtosecond laser plasma filament in air. Opt Commun. 2008;281:1268–74.

[20] Liu W, Bernhardt J, Théberge F, Chin SL, Châteauneuf M, Dubois J. Spectroscopic characterization of femtosecond laser filament in argon gas. J Appl Phys. 2007;102:33111.

[21] Mitryukovskiy S, Liu Y, Ding P, Houard A, Couairon A, Mysyrowicz A. Plasma luminescence from femtosecond filaments in air: Evidence for impact excitation with circularly polarized light pulses. Phys Rev Lett. 2015;114:63003.

[22] Itikawa Y. Cross sections for electron collisions with nitrogen molecules. J Phys Chem Ref Data. 2006;35:31.

[23] Zhao L, Wang R, Zhang S, Yang T, Lian Y. Ionization suppression of heteronuclear diatomic and triatomic molecules in strong infrared laser fields. Chin J Chem Phys. 2017;30:631–6.

[24] Pellerin S, Musiol K, Pokrzywka B, Chapelle J. Stark width of the 696.5 nm argon I line. J Phys B-At Mol Opt. 1996;29:3911.